Vehicle Posture Control through Aggressive Maneuvering for Mitigation of T-bone Collisions

Imon Chakraborty, Panagiotis Tsiotras, and Jianbo Lu

Abstract—This work analyzes the mitigation of unavoidable T-bone collisions between two automobiles through the execution of an aggressive maneuver involving a rapid yaw rotation of one of the vehicles, in order to achieve a favorable vehicle posture prior to the collision. The maneuvering vehicle is assumed to possess torque vectoring technology at the rear wheels, allowing the generation of a direct yawing moment. The maneuver is posed as an optimal control problem, whose numerical solution yields the optimal control strategy. Several conditions involving a variety of speeds and friction coefficients are investigated.

I. INTRODUCTION

Active safety systems such as ABS, TCS, ESP, AFS, etc ([1], [2], [3]) have become increasingly available on production vehicles, assisting the driver to avoid "abnormal" driving scenarios (skidding, excessive understeer/oversteer) that are characterized by nonlinear vehicle dynamics. They achieve this by restricting the operational envelope of the vehicle within a linear, stable regime. While this is a logical way to enhance vehicle stability, it is an overly conservative approach from the standpoint of vehicle controllability. There are instances, however, where the effect of a collision can be alleviated by deliberately operating the vehicle in the nonlinear regime through the controlled use of aggressive maneuvering. This work analyzes such a maneuver to avoid T-bone collisions, made possible by deliberately expanding the operational envelope of the vehicle.

T-bone collisions (Fig. 1,[4]), in which one vehicle rams the side of another, frequently occur when one vehicle violates a red light or stop sign and proceeds into a traffic intersection, where it collides with another vehicle traveling perpendicular to it. Such an incursion may be the result of a mechanical failure (stuck throttle, failed brakes), insufficient traction (wet/icy roads), lack of driver situational awareness, etc.

Even if the collision is physically unavoidable, its effects may be mitigated by applying intelligent control to at least one of the vehicles. In this work, we analyze an unavoidable T-bone collision scenario between two vehicles, under the assumption that the intelligent vehicle is mechanically sound, and sufficient road-tire traction exists to allow the execution of the proposed maneuver.

The maneuver involves a segment of maximum straight-line braking, followed by a rapid yaw rotation that brings the longitudinal axes of the two vehicles into a near parallel

Imon Chakraborty, MS student, Aerospace Engineering, Georgia Institute of Technology, Email: imonchakraborty@gatech.edu

Panagiotis Tsiotras, Professor, Aerospace Engineering, Georgia Institute of Technology, Email: tsiotras@gatech.edu

Jianbo Lu, Technical Specialist, Global Vehicle Dynamics, Driver Assistance and Active Safety Research and Advanced Engineering, Ford Motor Company, Email: jlu10@ford.com
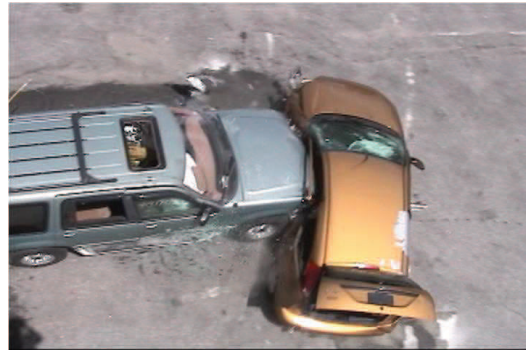

Fig. 1. T-bone collision.

alignment. Such a relative pre-impact orientation mitigates the effects of the collision by distributing the residual kinetic energy over a larger surface area. The tire force requirements and the braking inputs required to perform the first segment have been analyzed in [5] and [6] respectively. This work focuses on the rapid yaw rotation immediately following the straight-line braking segment. The execution of the proposed maneuver is facilitated by Torque Vectoring (TV) technology [7], which allows a "direct" yawing moment to be generated to complement the moment generated by front-wheel steering.

II. TORQUE VECTORING TECHNOLOGY

Torque Vectoring (TV) technology, described as "left-right torque vectoring" in [7], uses the concepts of Differential Braking (DB) and Active Differential (AD) in order to generate a direct yawing moment on the vehicle without affecting its longitudinal response. DB allows independent braking of all four wheels, thus allowing the generation of a yawing moment without any steering input. Currently available Electronic Stability Control (ESC) systems utilize this concept to augment directional stability and ensure controllability in conditions of reduced grip or driver-induced instability [8]. AD, on the other hand, incorporates an Electronic Control Unit (ECU) that uses information on yaw rate, lateral acceleration etc, to determine the necessary torque distribution to the left and right drive wheels to eliminate unwanted handling behavior (e.g., understeer). TV uses the concepts of DB and AD in tandem, to vector torque between the left and right wheels, such that a braking force is generated on one side while a tractive (driving) force of the same magnitude is generated on the other. As noted in [7], the direct yawing moment thus generated is independent of the engine torque output, and does not affect the vehicle's longitudinal acceleration/deceleration response. More crucially, since TV acts on both left and right wheels, it can generate a larger direct yawing moment than either DB or AD acting alone. Moreover, DB and AD acting alone may affect the vehicle longitudinal response. In this

paper we assume rear-axle TV only for two reasons: first, the steering mechanism makes front TV mechanically more complex to implement than rear TV. Second, rear-axle TV does not limit the driver's steerability, while for front-axle TV, large front braking will lead to a reduction of the cornering capacity of the front wheels which, in turn, will limit the driver's steering authority. Nonetheless, front-axle TV can also be applied, if desired, with the same presented methodology being applicable.

III. VEHICLE MODEL

Although some prior works [9], utilize a four-wheeled model, the "bicycle model," introduced in [10], is a commonly used simplification, which will also be used in this work. The left and right wheels are merged to yield a single-track "bicycle," consisting of a single front and rear tire. This representation is unable to capture certain aspects of the vehicle's dynamics such as lateral load transfer during cornering or the roll dynamics. However, with suitable modifications, the basic bicycle model can be modified to incorporate the effects of longitudinal load transfer ([11], [12]) and the friction circle constraint ([11], [12], [13]). In this work, longitudinal load transfer is not included, but the friction circle constraint is modeled, due to the nonlinear tire response encountered for high tire slip angles arising from aggressive yawing or drifting. The bicycle model, with relevant nomenclature and conventions, is shown in Fig. 2.

The vehicle's state vector is given by $\mathbf{x} = [u, v, r, \psi, x, y]^T$, where u, v are the components of the vehicle's total velocity V along the body-fixed x_b and y_b directions, i.e. $V = \sqrt{u^2 + v^2}$, r is the yaw rate, ψ is the heading, and x, y are the coordinates of the vehicle's CG measured from a fixed origin. The control vector is chosen as $\mathbf{u} = [\delta, F_{xf}, F_{xr}, M_d]^T$, featuring, respectively, the steering angle, the front and rear tire longitudinal forces and the direct yawing moment generated using TV. Other selections are also possible for the longitudinal control parameters, e.g., tire longitudinal slip ratio ([11], [12]), wheel torque or angular velocity. With the above state and control vectors, the equations of motion of the bicycle model are given below

$$\dot{u} = \frac{1}{m}(F_{xf}\cos\delta - F_{yf}\sin\delta + F_{xr}) + vr, \tag{1a}$$

$$\dot{v} = \frac{1}{m}(F_{xf}\sin\delta + F_{yf}\cos\delta + F_{yr}) - ur, \tag{1b}$$

$$\dot{r} = \frac{1}{I_z}(\ell_f(F_{xf}\sin\delta + F_{yf}\cos\delta) - \ell_r F_{yr} + M_d), \tag{1c}$$

$$\dot{\psi} = r, \tag{1d}$$

$$\dot{x} = u\cos\psi - v\sin\psi, \tag{1e}$$

$$\dot{y} = u\sin\psi + v\cos\psi. \tag{1f}$$

In (1), m and I_z are, respectively, the vehicle mass and moment of inertia. The vehicle's sideslip angle is defined as $\beta = \arctan(v/u) = \arctan(\dot{y}/\dot{x}) - \psi$, and the relations $u = V\cos\beta$ and $v = V\sin\beta$ hold. M_d is the direct yawing moment created as a result of TV. F_{i*} ($i = x, y; * = f, r$) denote the longitudinal and lateral forces developed at the front and rear tires, referred to a tire-fixed reference frame. These forces

depend on the normal loads on the front and rear axles, F_{zf} and F_{zr}. For this analysis, the latter are treated as equal to their steady-state (static) values as follows,

$$F_{zf} = \frac{mg\ell_r}{\ell_f + \ell_r}, \quad F_{zr} = \frac{mg\ell_f}{\ell_f + \ell_r}, \tag{2}$$

where ℓ_f and ℓ_r are the distances of the front and rear axles from the CG of the vehicle respectively, as shown in Fig. 2.
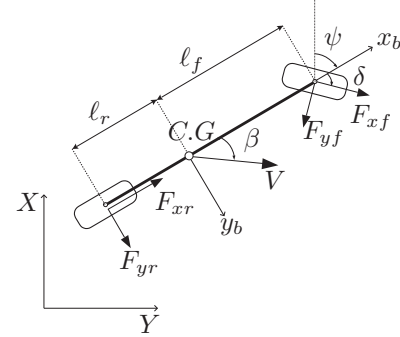

Fig. 2. Bicycle model.

Since the aggressive maneuver analyzed in this paper involves large slip angles, the linear force-slip relationships, such as those found in [14], [15] are not applicable. Third order polynomial [16] and rational function approximations [17] can capture the nonlinear tire dynamics and saturation effects, but in this work, the well-known Pacejka "Magic Formula" (MF) [18] is used instead. The MF models the tire forces as transcendental functions of the tire longitudinal and lateral slips. Using this representation, the lateral tire forces are expressed as

$$F_{y*} = -F_{y*}^{\max}\sin(C\arctan(Bs_{y*})), \quad * = f, r \tag{3}$$

where the constants B and C depend on the tire and road surface characteristics, and s_{yf} and s_{yr} are the lateral slip ratios of the front and rear tires, expressed as

$$s_{yf} = \frac{v\cos\delta - u\sin\delta + r\ell_f\cos\delta}{u\cos\delta + v\sin\delta + r\ell_f\sin\delta}, \tag{4a}$$

$$s_{yr} = \frac{v - \ell_r r}{u}. \tag{4b}$$

It should be noted that the maximum force a tire can extract from the ground is finite, and the maximum longitudinal and lateral forces that can be achieved at a given time are not mutually independent. These constraints are represented by the so-called "friction circle," ([11], [13]). In this work, a representation of the friction circle is utilized as follows:

$$F_{x*} \leq \mu F_{z*}, \quad * = f, r, \tag{5a}$$

$$F_{y*}^{\max} = \sqrt{(\mu F_{z*})^2 - F_{x*}^2}, \quad * = f, r. \tag{5b}$$

The conditions (5) together enforce the friction circle constraint.

The proposed rotation maneuver is performed subject to the following assumptions.

1) DB and AD act only on the rear axle.

2) The combined effect of DB and AD is to generate equal and opposite forces on the rear-left (RL) and rear-right (RR) tires, similarly, to the TV concept.
3) The driving and braking forces sent to the front and rear axle are distributed in the ratio $(1 - \gamma) : \gamma$, where $\gamma \in [0, 1]$.
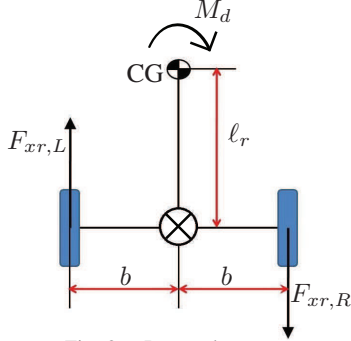4) The RL and RR tires see the same lateral slip angle.

Fig. 3.   Rear axle geometry.

Figure 3 shows the relevant geometry of the rear axle. Using this geometry subject to the previous assumptions, we have

$$M_d = (F_{xr,L} - F_{xr,R})b = 2bF_{xr,L}, \qquad (6)$$

where b is the semi-track width of the vehicle. From (6),

$$F_{xr,L} = M_d/(2b), \quad F_{xr,R} = -M_d/(2b), \quad F_{xr} = 0. \quad (7)$$

Using Assumptions 2 and 3, we also have

$$F_{xf} = \{(1-\gamma)/\gamma\}|F_{xr,L}| = \{(1-\gamma)/(2b\gamma)\}|M_d|. \quad (8)$$

Note that (8) implies that $F_{xf} \geq 0$, whose justification is provided later on. In order to compute $F_{yr}^{\max}$, the friction circle constraint for both the RL and RR tires must be considered separately. Using Assumptions 2), 3) and 4), the net rear-axle lateral force F_{yr} is given by

$$\begin{aligned} F_{yr} &= F_{yr,L} + F_{yr,R} \\ &= F_{yr}^{\max} \sin(C \arctan(Bs_{yr})), \end{aligned} \qquad (9)$$

where $F_{yr}^{\max} = F_{yr,L}^{\max} + F_{yr,R}^{\max} = \sqrt{(\mu F_{zr})^2 - (2F_{xr,L})^2}$. The tire lateral forces F_{yf} and F_{yr} are now computed by a direct application of (3), with Assumption 4) invoked for F_{yr}.

Note that both the RL and RR tires are saturated in the longitudinal direction when $|F_{xr,L}| = |F_{xr,R}| = \mu F_{zr}/2$. This yields $F_{yr}^{\max} = 0$, which when substituted in (9) gives $F_{yr} = 0$. Note also from (8) that F_{xf} is a function of the direct yawing moment M_d, and from (7) it follows that $F_{xr} = 0$, so the control vector in fact reduces to $\mathbf{u} = [\delta, M_d]^T$. In the current formulation of the problem, whereas M_d is assumed to be provided by a TV (DB/AD) system, the control input δ to the wheels can be provided either by the driver, or by an active steering system [19], [20], [21] that can compensate/override the driver's steering wheel input so that the optimally calculated amount of steering is applied to the front wheels.

Each of the control inputs δ and M_d is assumed to be constrained between some maximum and minimum values:

$$\delta_{\min} \leq \delta(t) \leq \delta_{\max}, \quad M_{d,\min} \leq M_d(t) \leq M_{d,\max} \quad (10)$$

The extreme steering deflection depends on the geometry of the steering system, and the maximum magnitude of the direct yawing moment M_d can be computed based on Fig. 3 and the principle of limiting friction. In particular,

$$M_{d,\max} = -M_{d,\min} = \mu F_{zr} b. \qquad (11)$$

Table I provides the values for all vehicle and tire parameters used in the numerical simulations.

TABLE I
VEHICLE DATA.

Variable	Value	Unit	Variable	Value	Unit
m	1450	Kg	B	7	-
I_z	2740	Kg.m^2	C	1.4	-
ℓ_f	1.1	m	$\delta_{\max}$=-$\delta_{\min}$	45	deg.
ℓ_r	1.6	m	g	9.81	m/s^2
b	0.75	m	γ	0.6	-

IV. QUALITATIVE DESCRIPTION OF THE MANEUVER

Intuitively speaking, the acceleration phase should involve pro-steering (steering in the direction of desired rotation) and the deceleration should involve counter-steering. Also, intuitively, the direct yawing moment vector should be in the same direction as the angular acceleration vector. It should be noted that during the course of the rotation, the front tire is always driven according to a fixed ratio to the driven rear tire (left or right), and never braked, i.e., $F_{xf} \geq 0$. Assuming a clockwise rotation as viewed from above, the pro-steering phase involves a steering deflection to the right ($\delta > 0$). Since initially there is no lateral velocity or yaw rate, this gives $F_{yf} \geq 0$. If at this time the front wheel was braked, (i.e., if $F_{xf} < 0$), it is clear from the vehicle geometry (Fig. 2) that the moment due to F_{xf} would have opposed that due to F_{yf}. In other words, braking would have partly negated the moment generated through steering input, and thus adversely affected the yaw acceleration. For the yaw deceleration/arrest phase, counter-steering implies $\delta < 0$ which, depending on the vehicle's lateral velocity and yaw rate, may yield $F_{yf} < 0$. In this case also, the moment generated by braking the front tire opposes that generated by the lateral force of the front tire, F_{yf}. For this reason, the condition $F_{xf} \geq 0$ is maintained for the duration of the maneuver. Furthermore, by avoiding braking of the front wheels the driver maintains the necessary steering control.

V. OPTIMAL CONTROL PROBLEM FORMULATION

Consider the nonlinear dynamical system (1) subject to the force modeling conditions given by (2)-(9), and controlled by $\mathbf{u} = [\delta, M_d]^T$, subject to the control constraints (10). The system is to be transferred from an initial state given by $\mathbf{x}_0 = [u_0, v_0, r_0, \psi_0, x_0, y_0]^T = [V_0, 0, 0, 0, 0, 0]^T$ to a final state given by $\mathbf{x}_f = [u_f, v_f, r_f, \psi_f, x_f, y_f]^T$, where $r_f = 0$ and $\psi_f = \pi/2$, while minimizing the cost function given by

$$\mathcal{J} = \int_0^{t_f} \mathrm{d}t = t_f. \qquad (12)$$

In other words, the rotation is posed as a minimum-time optimal control problem (OCP). Subsequent extensions to this work will consider the problem of limiting the lateral deviation encountered during the performance of the maneuver, by adding a term to the cost function that penalizes final lateral deviation. In this case, (12) becomes $\mathcal{J} = t_f + \kappa y_f^2$ for $\kappa > 0$.

VI. NUMERICAL SOLUTION OF THE OCP

Given the high degree of nonlinearity present in the vehicle system dynamics, a numerical solution to the optimal control problem was obtained using *Gauss Pseudospectral Optimization Software* (GPOPS) [22], which requires guesses for the initial and final times, states and controls to perform the optimization. The optimality of the obtained solution was verified from the time histories of the Hamiltonian and the co-states of the problem, also computed by GPOPS, but these are not shown in the paper in the interest of brevity. Conformity with (10) was used to ensure control feasibility.

VII. RESULTS AND DISCUSSION

The maneuver was analyzed for different initial velocities and tire-road coefficients of friction. Table II provides a description of each case tested.

TABLE II
CASE DESCRIPTIONS

Case	Initial Speed V_0, km/h	Friction coeff., μ	Case	Initial Speed V_0, km/h	Friction coeff., μ
1	40	0.80	4	40	0.50
2	55	0.80	5	55	0.50
3	72	0.80	6	72	0.50

Note that Cases 1-3 consider three initial velocities with a high coefficient of friction, which is meant to represent contact between an average tire and a level, dry road free from any loose material. Cases 4-6 analyze the same three initial velocities with a lower coefficient of friction, which is meant to represent a wet road surface.

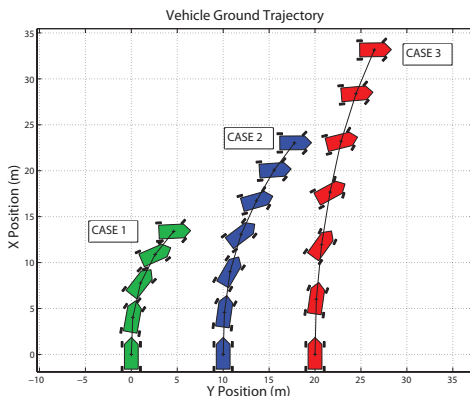### A. Cases 1, 2, and 3: Dry Asphalt

Fig. 4.   Ground Trajectories - Case 1, 2, and 3

The minimum-time solutions for Cases 1, 2, and 3 on dry asphalt were computed respectively as 1.62 sec, 1.81 sec, and 1.90 sec. Figure 4 shows the trajectories followed by the vehicle during the maneuver for Cases 1, 2, and 3. Note that as the initial velocity increases from Case 1 to

Case 3, the X-distance traversed before the completion of the rotation is higher. Also, note that since only the minimum-time problem is dealt with, the vehicle in each case goes through a lateral deviation as well. Subsequent extensions will focus on limiting this lateral deviation, since the ultimate goal is to be able to perform the collision mitigation maneuver within the dimensions of an average traffic intersection.
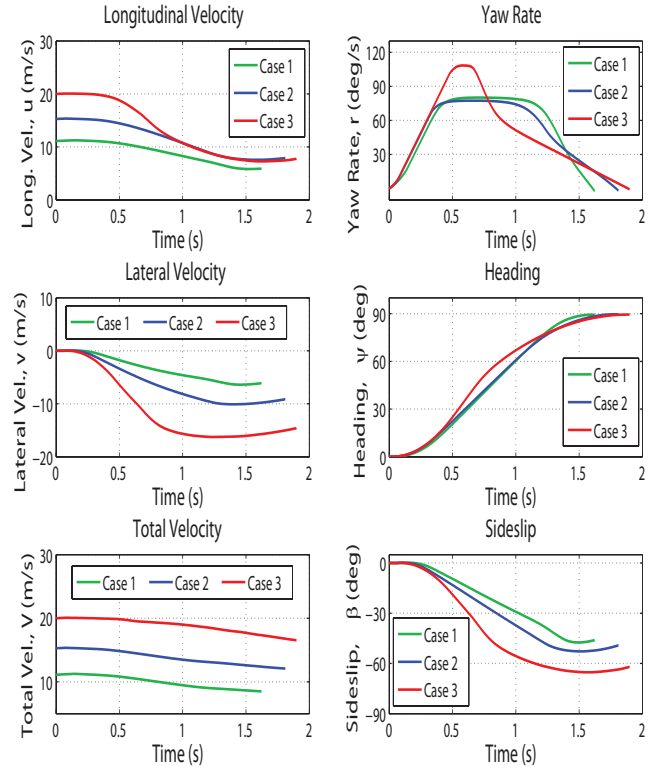

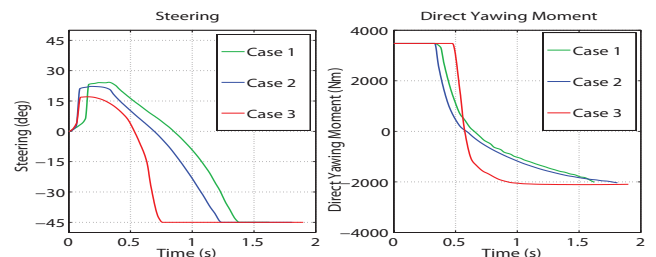Fig. 5.   State histories - Case 1, 2, and 3.

Fig. 6.   Control histories - Case 1, 2, and 3.

Figure 5 shows a comparison of the evolution of the vehicle states during the course of the maneuver for Cases 1, 2, and 3. It is observed that the highest yaw rate is achieved for Case 3, where the initial velocity is the highest. This case also results in a larger sideslip angle than the other cases. Figure 6 shows the control histories for Cases 1, 2 and 3. Note that for each case, the direct yawing moment is at its positive extreme at the start of the maneuver, while the steering deflection is at its negative extreme (full counter-steer) towards the end of the maneuver. Note that since Cases 1-3 all involve the same coefficient of friction, the maximum magnitude of the direct yawing moment is the same for all three cases. Figure 7 shows the longitudinal and lateral forces generated by the front and rear tires during the maneuver for Cases 1-3. Note
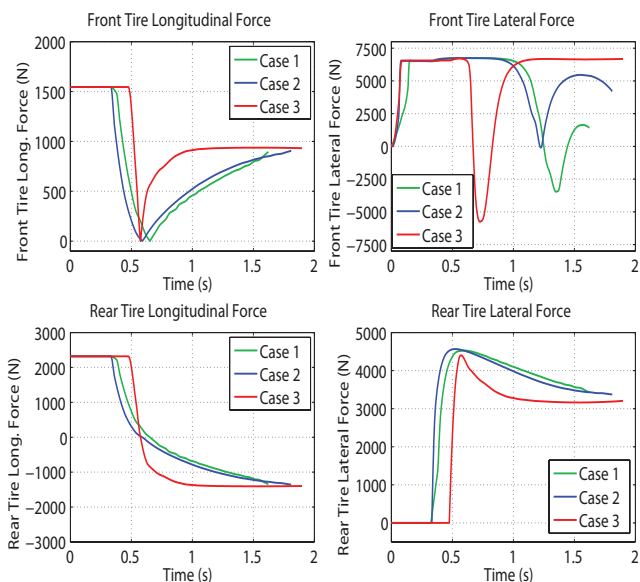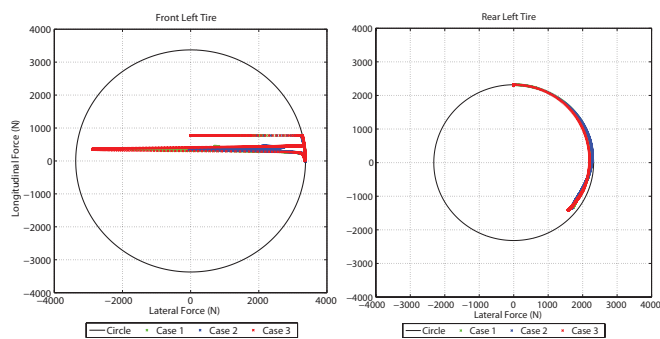
Fig. 7.   Tire forces - Case 1, 2, and 3.

(a) Front Left Tire.   (b) Rear Left Tire.

Fig. 8.   Tire operating conditions - Case 1, 2, and 3. Only the left front and rear tires are shown, as the forces on the right tires can be immediately inferred from those.

that according to the formulation of the vehicle model, the front tires are driven in a fixed force ratio to the driven rear tire, and the condition $F_{xf} \geq 0$ always holds. This is evident from the plots of the front and rear tire longitudinal forces.

The plot for the front tire lateral force (Fig. 7) clearly shows pro-steering and counter-steering yawing moments generated by the steering input. However, towards the end of the maneuver, when the sideslip angle is larger, the lateral force generated by the front tire opposes the yaw deceleration despite full counter-steering input.

The plot for the rear-left (RL) tire lateral force (Fig. 7) shows that for each case the rear tire is initially saturated along the longitudinal direction, and is thus unable to generate a lateral force (note: the rear-right (RR) tire longitudinal force is the negative of that for the RL tire, and thus it is not shown). For the rest of the maneuver, the rear tire lateral force acts opposite to the direction of the slide, i.e., to the right, viewed from the vehicle's body-fixed frame.

Figure 8 shows the friction circle superimposed on the left tire forces for Cases 1-3, and represents the tire operating conditions. For brevity, only the left front and rear tire forces

are shown, since the right front and rear tire forces can be immediately obtained from the left tire forces using the tire constraint relationships mentioned in Section III. It is seen that the rear tires operate at or close to saturation for the duration of the maneuver, with both longitudinal and lateral saturation being encountered. The front tires are driven by a fixed ratio to the driven rear tire and have a friction circle with a larger radius (on the account of the higher normal force on the front axle), and hence these do not encounter longitudinal saturation. However, lateral saturation is encountered during the rotation. These observations reinforce the necessity of using nonlinear tire modeling for these types of maneuvers.

TABLE III
OPTION WINDOWS FOR CASES 1, 2, AND 3

Case	Speed (Km/h)	Stopping dist. (m)	Rotation dist. (m)	Option Window (m)
1	40	26	15	11
2	55	41	24	17
3	72	60	35	25

TABLE IV
RECOMMENDED ACTIONS FOR CASES 1, 2, AND 3

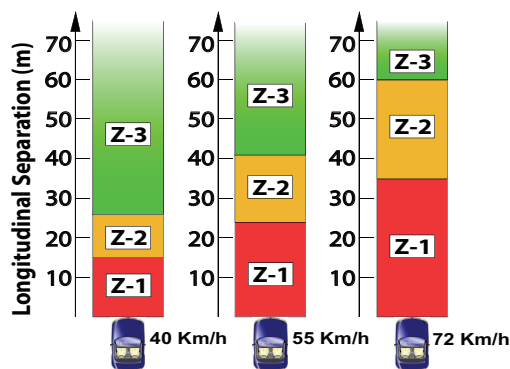| Zone	Braking to stop	90 deg. Rotation	Recommended Action
Z-1	Impossible	Impossible	Rotate
Z-2	Impossible	Possible	Rotate
Z-3	Possible	Possible	Brake

Fig. 9.   Decision making options.

The results obtained for Cases 1-3, in conjunction with accepted values of required stopping distances from various initial speeds, allow a decision-making strategy to be superimposed on the collision mitigation/avoidance problem, where the recommended action depends on the distance between the intelligent vehicle and the second vehicle, when the latter is sighted and classified as a collision threat.

Table III shows the stopping distances required from initial speeds of 40 km/h (Case 1), 55 Km/h (Case 2), and 72 Km/h (Case 3). These figures are from the Virginia Code - Tables of Speed and Stopping Distances (46.2-880) [23], and apply to vehicles in good condition on a level, dry road free from loose material. The same table also shows the X-distance traversed during the rotation for each of Cases 1, 2, and 3. It is clear that in each case the X-distance traversed during the aggressive rotation is less than the distance required to brake to a full stop in a straight line. This results in the creation of an "option

window" (Zone Z-2 in Fig. 9), such that if the second vehicle is spotted within this window, a successful 90 deg rotation is possible, although braking to a full stop using straight-line braking is not.

In addition to zone Z-2, Table IV shows the recommended actions for the other two zones which arise, namely Z-1 and Z-3. It should be noted that zone Z-1 allows neither successful braking nor successful rotation, while Z-3 poses no real threat as simple straight-line braking will suffice. Figure 9 also shows the relative positions and lengths of the zones for the three speeds considered.

B. Cases 4, 5, and 6: Wet Asphalt

The results for the wet asphalt (Cases 4, 5, and 6) are shown in Fig. 10. Only the vehicle trajectories are shown owing to lack of space. Because of the lower friction coefficient, the X-distance traversed during the rotation for each case is higher than the corresponding distance with the higher friction coefficient. The minimum-time solutions for Cases 4, 5, and 6 are respectively 2.22 sec., 2.40 sec., and 2.40 sec.
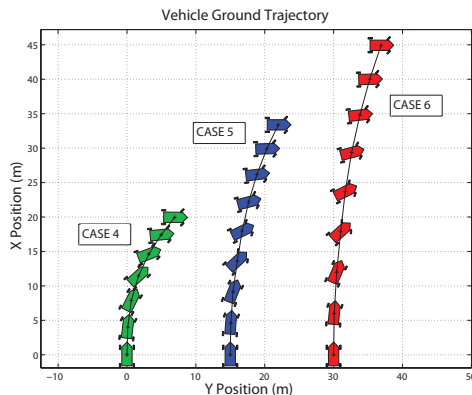

Fig. 10. Ground trajectories - Case 4, 5, and 6.

VIII. Conclusion

Torque vectoring (TV) technology is used in a novel manner to perform an aggressive maneuver aimed at mitigating a T-bone collision. The maneuver is posed as an optimal control problem and solved numerically, and the solution is validated using a nonlinear model of the vehicle. The creation of "option zones" due to the performance of the aggressive rotation is described and explained for various initial speeds. Future work includes the incorporation of the effects of longitudinal load transfer and the use of conventionally available steering and braking controls to produce these aggressive manuevers (i.e., without torque-vectoring). Finally, the real-time computation of such aggressive trajectories on board the vehicle also poses a challenge with the current state of technology and needs to be dealt with before implementation on an actual vehicle is possible.

References

[1] M. Yamamoto, "Active control strategy for improved handling and stability," *SAE Transactions*, vol. 100, no. 6, pp. 1638–1648, 1991.

[2] F. Assadian and M. Hancock, "A comparison of yaw stability control strategies for the active differential," in *Proc. IEEE Int. Symp. Industrial Electronics ISIE 2005*, vol. 1, 2005, pp. 373–378.

[3] A. T. van Zanten, "Evolution of electronic control system for improving the vehicle dynamic behavior," in *Advanced Vehicle Control Conference (AVEC)*, Hiroshima, Japan, 2002.

[4] Cedarbyrne Consulting Services - Accident Reconstruction Specialists, Web: www.cedarbyrne.com.

[5] H. Peng and J. Hu, "Traction/braking force distribution for optimal longitudinal motion during curve following," *Vehicle System Dynamics*, vol. 26, no. 4, pp. 301–320, October 1996.

[6] P. Tsiotras and C. Canudas deWit, "On the optimal braking of wheeled vehicles," in *American Control Conference*, Chicago, IL, June 28-30 2000, pp. 569–573.

[7] K. Sawase, Y. Ushiroda, and T. Miura, "Left-right torque vectoring technology as the core of super all wheel control (S-AWC)," Mitsubishi Motors, Tech. Rep. 18, 2006.

[8] L. Anders, T. Claes, M. Krafft, and K. Anders, "The effectiveness of electronic stability control (ESC) in reducing real life crashes and injuries," *Traffic Injury Prevention*, vol. 7, pp. 38–43, 2006.

[9] J. Edelmann and M. Plochl, "Handling characteristics and stability of the steady-state powerslide motion of an automobile," *Regular and Chaotic Dynamics*, vol. 14, no. 6, pp. 682–692, 2009.

[10] P. Riekert and T. Schunck, "Zür fahrmechanik des gummibereiften kraftfahrzeugs," *Ingenieur Archiv*, vol. 11, pp. 210–224, 1940.

[11] E. Velenis, E. Frazzoli, and P. Tsiotras, "Steady-state cornering equilibria and stabilization for a vehicle during extreme operating conditions," *International Journal of Vehicle Autonomous Systems*, vol. 8, pp. 217–241, 2010.

[12] E. Velenis, P. Tsiotras, and J. Lu, "Modeling aggressive maneuvers on loose surfaces: The cases of trail-braking and pendulum turn," in *European Control Conference*, Kos, Greece, July 2-5 2007.

[13] R. Y. Hindiyeh and J. C. Gerdes, "Equilibrium analysis of drifting vehicles for control design," in *Proceedings of the ASME 2009 Dynamic Systems and Control Conference*, Hollywood, California, USA, October 12 - 14, 2009 2009.

[14] D. Smith and J. Starkey, "Effects of model complexity on performance of automated vehicle steering controllers: Model development, validation and comparison," *Vehicle System Dynamics*, vol. 24, no. 2, pp. 163–181, 1995.

[15] J. Hilgert, K. Hirsch, T. Bertram, and M. Hiller, "Emergency path planning for autonomous vehicles using elastic band theory," in *Proceedings of the 2003 IEEE/ASME International Conference on Advanced Intelligent Mechatronics*, 2003.

[16] B. Badji, E. Fenaux, M. E. Bagdouri, and A. Miraoui, "Nonlinear single track model analysis using Volterra series approach," *Vehicle System Dynamics*, vol. 47, no. 1, pp. 81–98, January 2009.

[17] S. C. Baslamisli, I. E. Kose, and G. Anlas, "Gain-scheduled integrated active steering and differential control for vehicle handling improvement," *Vehicle System Dynamics*, vol. 47, no. 1, pp. 99–119, January 2009.

[18] E. Bakker, L. Nyborg, and H. Pacejka, "Tyre modeling for use in vehicle dynamics studies," in *SAE Paper No. 870421*, 1987.

[19] O. Mokhiamar and M. Abe, "Active wheel steering and yaw moment control combination to maximize stability as well as vehicle responsiveness during quick lane change for active vehicle handling safety," *Proceedings of the Institution of Mechanical Engineers, Part D: Journal of Automobile Engineering*, vol. 216, no. 2, pp. 115–125, 2002.

[20] S. Di Cairano and H. E. Tseng, "Driver-assist steering by active front steering and differential braking: Design, implementation and experimental evaluation of a switched model predictive control approach," in *Proc. 49th IEEE Conf. Decision and Control (CDC)*, 2010, pp. 2886–2891.

[21] B. Tongue, "Two brains, one car - actively controlled steering," *IEEE Control Systems Magazine*, vol. 25, no. 5, pp. 14–17, 2005.

[22] A. Rao, D. Benson, G. Huntington, C. Francolin, C. Darby, M. Patterson, and I. Sanders, *User's Manual for GPOPS Version 3.0: A MATLAB Software for Solving Multiple-Phase Optimal Control Problems using Psuedospectral Methods*.

[23] Code of Virginia, Tables of Speed and Stopping Distances, Motor Vehicles, Title 46.2-880, Web: http://leg1.state.va.us/cgi-bin/legp504.exe?000+cod+46.2-880.